Three-Dimensional Radiative Heat-Transfer Solutions by the Discrete-Ordinates Method

W. A. Fiveland*
Babcock & Wilcox Company, Alliance, Ohio

Radiative heat transfer in a three-dimensional participating medium was predicted using the discrete-ordinates method. The discrete-ordinates equations are formulated for an absorbing, anisotropically scattering, and re-emitting medium enclosed by gray walls. The solution strategy is discussed and the conditions for computational stability are presented. Several test enclosures are modeled. Results have been obtained for the S2, S4, S6, and S8 approximations that correspond to 8, 24, 48, and 80 fluxes, respectively, and are compared with the exact-zone solution and the P3 differential approximation. Solutions are found for conditions that simulate absorbing media and isotropically and anisotropically scattering media. Solution accuracy and convergence are discussed for the various flux approximations. The S4, S6, and S8 solutions compare favorably with the other methods and can be used to predict radiant intensity, incident energy, and surface heat flux.

Nomenclature

A	= north-south areas, m^2
a_n	= coefficients of a Legendre series
b_n	= coefficients of a modified Legendre series
B	= east-west areas, m^2
C	= front-back areas, m^2
E	= emissive power ($=\bar{\sigma}T^4$), W/m^2
G	= incident energy, $\int_{4\pi} I\,d\Omega$, W/m^2
I	= radiant intensity, $W/(m^2 \cdot Sr)$
L	= enclosure dimension, m
$\boldsymbol{n}$	= unit normal
q	= heat flux, W/m^2
$\boldsymbol{r}$	= position vector, m
S	= source term, W/m^3
$\forall_p$	= volume of pth control volume, m^3
w_m	= weight function in a direction $-m$ (fractional area of a unit sphere)
x	= coordinate, m
y	= coordinate, m
z	= coordinate, m
α	= finite-difference weighting factor
β	= extinction coefficient, $\sigma + \kappa$, m^{-1}
ϵ	= surface emittance
κ	= absorption coefficient, m^{-1}
μ,ξ,η	= ordinates $\mu = \cos\Theta$, $\xi = \sin\Theta \sin\phi$, $\eta = \sin\Theta \cos\phi$
Ω	= outgoing direction of radiation
Φ	= phase function
ρ	= surface reflectance
σ	= scattering coefficient, m^{-1}
$\bar{\sigma}$	= Boltzmann's constant, 5.669×10^{-8} $W/(m^2 \cdot K^4)$
Θ	= angle between incoming and outgoing intensity
∇	= gradient/vector

Superscripts

$(\,)'$	= incoming value
m'	= incoming direction

Subscripts

b	= blackbody
g	= gas
m	= outgoing ordinate direction
m'	= incoming ordinate direction
$N,S,E,W,$ F,B	= node points around p
$n,s,e,w,$ f,b	= control volume faces surrounding node point p
p	= control volume center
R	= radiative
x	= coordinate direction
y	= coordinate direction
z	= coordinate direction

Received Jan. 15, 1987; revision received Oct. 5, 1987.

*Research and Development Division, Alliance Research Center. Member AIAA.

Introduction

In many combustion devices, radiant heat transfer is the dominant mode of energy transfer. Accurate solutions of the performance of these devices are strongly linked to the solutions of the radiative transport equation (RTE).

Although a variety of computational tools have been proposed in the past several decades, recent advances in combustion modeling[1,2] have re-emphasized several important needs for radiative heat-transfer calculations. Current numerical modeling schemes require calculational tools that are efficient and integrate easily with the other transport equations based on finite-difference approaches. Moreover, in large-scale industrial and utility pulverized coal combustion furnaces, heat transfer is mainly by radiation. Radiation is attenuated not only by absorbing gases such as water vapor and carbon dioxide, but by suspended particulates (coal, char, ash, and soot). Accurate simulation of the radiative processes requires analysis of the combined absorption and scattering of radiant energy.

An extensive survey of multidimensional radiative models has been reported elsewhere.[3] Exact formulations for absorbing, emitting, and scattering media in rectangular enclosures have been documented.[4,5] "Exact" numerical solutions of the radiative transport equation can also be obtained with the Monte Carlo[6] and the zone methods.[7] The Monte Carlo technique is time consuming and the zone method is not easily adapted for problems involving scattering. Lockwood and Shah[8] have proposed a hybrid approach called the discrete-transfer method that has many characteristics of the Monte Carlo and flux methods, but is not easily implemented for radiative scattering. Menguc and Viskanta[9] recently presented a P3 approximation of the three-dimensional radiative transport equation. While this method treats absorption and scattering problems easily, it is still time consuming, and improving solution accuracy (P5) requires a laborious rederivation of the governing equations.

One approach that has received little attention in the heat-transfer community is the discrete-ordinates method, which can be applied to multidimensional problems involving absorption, scattering, and re-emission of energy. The discrete-ordinates method has been developed by a number of researchers,[10-12] but applied to radiative heat-transfer problems on a limited basis.[13-15] The method has been actively developed for the solution of the Neutron transport equation and, even though computational methods exist for those applications,[16] the computational methods apply to only a very limited number of radiative heat-transfer problems. Recent work by Khalil and Truelove[13] discusses use of the S4 discrete-ordinates approximation for a furnace application, but provides no insight on the accuracy, stability, or convergence characteristics of the method. Other work by Truelove is cited in Ref. 13, but is contained in proprietary laboratory reports. Fiveland[14,15] illustrated the flexibility of the discrete-ordinates method for a constant property cylindrical medium and a two-dimensional rectangular medium.

The current work applies the discrete-ordinates method to three-dimensional problems involving absorption and scattering and examines the method for radiative heat-transfer problems in more detail than previously done. A control volume formulation, which is based on the SN discrete-ordinates method and integrates well with other finite-difference methods,[12] is used with fully symmetric quadrature sets[17] defining the ordinate directions. The formulation permits usage of different flux approximations (e.g., ordinate directions) without reformulating the method. Solutions are benchmarked with exact zone solutions and a P3 approximation. Wall heat flux, emissive power, and temperature are predicted for the SN (S2, S4, S6, and S8) methods. Solution stability, accuracy, and computational times are discussed for the various SN solutions.

Analysis

Radiative Transport Equation

Consider the radiative transfer equation for the enclosure shown in Fig. 1. The balance of energy passing in a specified direction Ω through a small differential volume in an emitting-absorbing and scattering medium can be written as

$$(\Omega\cdot\nabla)I(\boldsymbol{r},\Omega) = -(\tilde{\kappa}+\tilde{\sigma})I(\boldsymbol{r},\Omega) + \tilde{\kappa}I_b(\boldsymbol{r}) + \frac{\tilde{\sigma}}{4\pi}\int_{\Omega'=4\pi} I(\boldsymbol{r},\Omega')\Phi(\Omega'\to\Omega)\,d\Omega' \tag{1}$$

where $\Phi(\Omega'\to\Omega)$ is the phase function of energy transfer from the incoming direction Ω' to the outgoing direction Ω (see Fig. 1); $I(\boldsymbol{r},\Omega)$ is the radiation intensity, which is a function of position and direction; $I_b(\boldsymbol{r})$ is the intensity of a blackbody radiation at the temperature of the medium; and $\tilde{\kappa}$ and $\tilde{\sigma}$ are the absorption and scattering coefficients of the medium, respectively. The expression of the left-hand side represents the gradient of the intensity in the specified direction Ω. The three terms on the right represent the changes in intensity due to absorption and outscattering, emission and inscattering, respectively.

Boundary Conditions

If the surface bounding the medium is assumed to emit and reflect diffusely, then the radiative boundary condition for Eq. (1) is given by

$$I(\boldsymbol{r},\Omega) = \epsilon I_b(\boldsymbol{r}) + \frac{\rho}{\pi}\int_{\boldsymbol{n}\cdot\Omega'<0} |\boldsymbol{n}\cdot\Omega| I(\boldsymbol{r},\Omega')\,d\Omega' \tag{2}$$

where $I(\boldsymbol{r},\Omega)$ is the intensity of radiant energy leaving a surface at a boundary location, ϵ the surface emissivity, ρ the surface reflectivity, and $\boldsymbol{n}$ the unit normal vector at the boundary location.

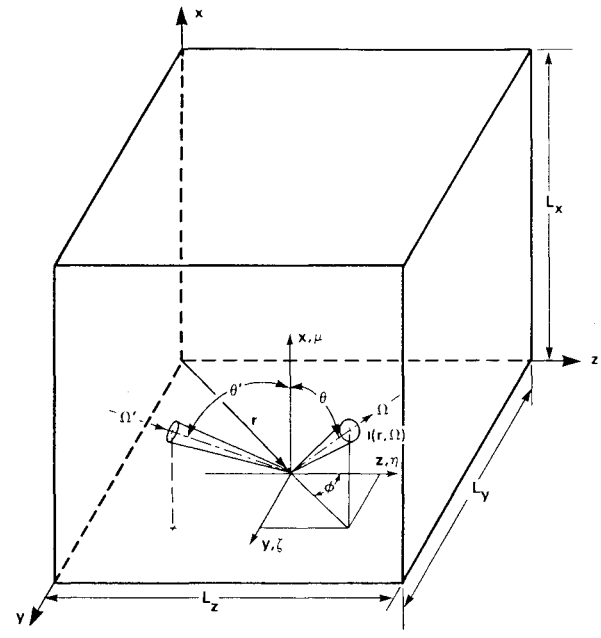

Fig. 1 Coordinate system.

The terms on the right-hand side of Eq. (2) represent contributions to the outgoing intensity due to emission from the surface and reflection of incoming radiation.

Phase Function

The phase function $\Phi(\Omega'\to\Omega)$, defined in Eq. (1), is the fraction of energy scattered into the outgoing direction Ω from the incoming direction Ω'. The phase function can be represented as a Legendre series,

$$\Phi(\Theta) = \sum_{n=0}^{N} (2n+1)\,a_n P_n(\cos\Theta) \tag{3}$$

where $\cos\Theta = \cos\theta\cos\theta' + \sin\theta\sin\theta'\cos(\phi-\phi')$ measures the angle Θ between the incident and outgoing beams (see Fig. 1). Using the spherical geometry, we can redefine

$$\cos\Theta = \mu\mu' + \xi\xi' + \eta\eta' \tag{4}$$

The phase function, defined by Eq. (3), is quite complex and the delta function approximation[18,19] can be used to approximate the forward spike. This spike occurs when radiative energy is highly forward scattered from micron-sized particles like coal, char, and fly ash. The approximation is written as

$$\Phi(\Theta,\Theta',\phi,\phi') = 2f\delta(1-\cos\Theta) + (1-f)\sum_{n=0}^{M}(2n+1)\,b_n P_n(\cos\Theta) \tag{5}$$

The relationship between the coefficients in Eqs. (3) and (5) can be found using the orthogonality of the Legendre polynomials to obtain

$$f = a_{M+1} \tag{6}$$

$$b_n = \frac{a_n - f}{1-f} \quad \text{for } n = 0,1,\ldots,M \tag{7}$$

The phase function [Eq. (5)] can be substituted into Eq. (1) with the result that the same form of Eq. (1) is obtained,

$$\Omega \cdot \nabla I(r,\Omega) = -\beta I(r,\Omega) + \kappa I_b(r) + \frac{\sigma}{4\pi}\int_{\Omega'=4\pi}\sum_{n=0}^{M}(2n+1)\,b_n P_n(\cos\Theta)\,I'(r,\Omega')\,d\Omega' \quad (8)$$

except the absorption and scattering coefficients can be written as

$$\kappa = \tilde{\kappa} \quad (9)$$

$$\sigma = (1-f)\,\tilde{\sigma} \quad (10)$$

where $\beta = \kappa + \sigma$.

Discrete-Ordinate Equations

Chandrasekhar[10] has described derivations of the discrete-ordinate equations for one-dimensional radiative transfer. For the multidimensional case, the radiative transport equation is also solved for a number of ordinate directions, with the integrals replaced by a quadrature summed over the ordinate directions. The RTE can be written

$$\mu_m\frac{\partial I^m}{\partial x} + \xi_m\frac{\partial I^m}{\partial y} + \eta_m\frac{\partial I^m}{\partial z} = -\beta I^m + \kappa I_b + \frac{\sigma}{4\pi}S_m \quad (11)$$

For a discrete direction Ω_m, the values μ_m, ξ_m, and η_m are the direction cosines of Ω_m. The angular integral, denoted S_m in Eq. (11), can be approximated as

$$S_m = \sum_{m'} w_{m'}\sum_{n=0}^{M}(2n+1)\,b_n P_n(\cos\Theta)\,I^{m'} \quad (12)$$

where the values m' denote incoming directions. The directions $\Omega_{m'}$ are pictured as a point on the surface of a unit sphere to which a surface area ($w_{m'}$) is associated. The quadrature scheme based on the moment-matching method[17] is used throughout. Equation (12) can be expanded by using Eq. (4) to obtain

$$S_m = \sum_{m'} w_{m'}\Phi(m',m)\,I^{m'} \quad (13)$$

where

$$\Phi(m',m) = \sum_{n=0}^{M}(2n+1)\,b_n P_n(\mu_m\mu_{m'} + \xi_m\xi_{m'} + \eta_m\eta_{m'}) \quad (14)$$

For the approximation ($M = 0$), the phase function is represented by a forward-directed delta function and an isotropic term, with $b_0 = 1.0$. Using the delta-Eddington approximation ($M = 1$), the parameters f, b_0, and b_1 replace the phase function by the sum of a forward-directed delta function and the linear anisotropic function $1 + 3b_1(\mu\mu_{m'} + \xi\xi_{m'} + \eta\eta_{m'})$. Thus, given the ordinate directions and the coefficients b_n, the function $\Phi(m', m)$ can be computed once.

The conditions on the boundary can be written as

$$I^m = \epsilon I_b + \frac{\rho}{\pi}\sum_{\substack{m'\\ \mu_{m'}<0}} w_{m'}|\mu_{m'}|I^{m'} \qquad x = 0 \quad (15)$$

$$I^m = \epsilon I_b + \frac{\rho}{\pi}\sum_{\substack{m'\\ \mu_{m'}>0}} w_{m'}|\mu_{m'}|I^{m'} \qquad x = L_x \quad (16)$$

$$I^m = \epsilon I_b + \frac{\rho}{\pi}\sum_{\substack{m'\\ \xi_m<0}} w_{m'}|\xi_{m'}|I^{m'} \qquad y = 0 \quad (17)$$

$$I^m = \epsilon I_b + \frac{\rho}{\pi}\sum_{\substack{m'\\ \xi_m>0}} w_{m'}|\xi_{m'}|I^{m'} \qquad y = L_y \quad (18)$$

$$I^m = \epsilon I_b + \frac{\rho}{\pi}\sum_{\substack{m'\\ \eta_m<0}} w_{m'}|\eta_{m'}|I^{m'} \qquad z = 0 \quad (19)$$

$$I^m = \epsilon I_b + \frac{\rho}{\pi}\sum_{\substack{m'\\ \eta_m>0}} w_{m'}|\eta_{m'}|I^{m'} \qquad z = L_z \quad (20)$$

In Eqs. (15–20), the second term on the right side of the equations represents the reflected incoming radiative heat flux, where the summations extend only over the incoming directions.

Finite-Difference Equations

The finite-difference form of the radiative transport equation can be obtained by integrating over the control volume shown in Fig. 2,

$$\mu_m A(I_e^m - I_w^m) + \xi_m B(I_n^m - I_s^m) + \eta_m C(I_f^m - I_b^m) = -\beta\forall_p I_p^m + \kappa\forall_p I_{bp} + \forall_p\frac{\sigma}{4\pi}\sum_{m'} w_{m'}\Phi_{m'm}I_p^{m'} \quad (21)$$

The intensities at each face of the control volume can be related to the cell-center intensity by the following relationships[12]:

$$I_p^m = \alpha I_n^m + (1-\alpha)I_s^m = \alpha I_e^m + (1-\alpha)I_w^m = \alpha I_f^m + (1-\alpha)I_b^m \quad (22)$$

Then, Eqs. (22) are used to eliminate the unknowns at the east, north, and front cell faces and gives rise to the finite-difference equation,

$$I_p^m = \frac{\mu_m A I_w^m + \xi_m B I_s^m + \eta_m C I_b^m + \alpha(S_1 + S_2)\forall_p}{\mu_m A + \xi_m B + \eta_m C + \alpha\beta\forall_p} \quad (23)$$

The quantities can be defined: $A = \Delta y\Delta z$, $B = \Delta x\Delta z$, and $C = \Delta x\Delta y$, where

$$S_1 = \kappa I_b$$

$$S_2 = \frac{\sigma}{4\pi}\sum_{m'} w_{m'}\Phi_{m'm}\,I_p^{m'}$$

Equation (23) is valid when the direction cosines are positive. Lathrop's[12] diamond-difference scheme is obtained if $\alpha = \frac{1}{2}$

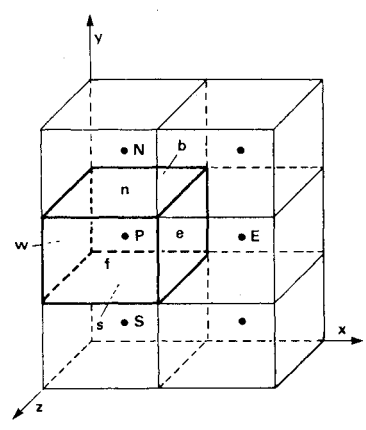

Fig. 2 Control volume.

and is globally second-order accurate. First-order finite-difference methods are obtained for $\frac{1}{2} < \alpha \leq 1$.

Solution of Discrete-Ordinate Equations

Solutions of Eq. (23) for each of the m directions are iterative, because the in-scattering source term and the boundary conditions depend on the intensity. The equations are solved by point-by-point iteration. To preserve numerical stability with the positive and negative direction cosines, Eq. (23) is rewritten as

$$I_p^m = \frac{|\mu_m| A I_{xr}^m + |\xi_m| B I_{yr}^m + |\eta_m| C I_{zr}^m + \alpha S \forall_p}{|\mu_m| A + |\xi_m| B + |\eta_m| C + \alpha \beta \forall_p} \tag{24}$$

with

$$I_p^m = \alpha I_{ie}^m + (1-\alpha) I_{ir}^m \tag{25}$$

where the subscript index i denotes the coordinate directions x, y, and z. The points in the computational domain are visited according to the direction that the radiation beam propagates—the beam has the same sense as the direction cosines. In Eqs. (24) and (25), subscripts e and r denote the end- and reference-face values of a computational cell and subscripts x, y, and z denote coordinate directions. For a positive set of direction cosines $(\mu_{m'}, \xi_{m'}, \eta_{m'})$, the end-face subscripts are defined by the values (e, n, f) and the reference-face subscripts are defined by the values (w, s, b). If the x and y ordinate values are positive with a negative z ordinate, the sweep proceeds in a way that the end- and reference-face subscripts are defined as (e, n, b) and (w, s, f), respectively. For an ordinate direction, therefore, the node intensity at point P is predicted using Eq. (24) with the proper reference-face intensities. The end-face intensities are then extrapolated using Eq. (25).

The modeled geometry is subdivided into a number of control volumes. Calculations are initiated by assuming the boundaries are radiatively black and the in-scattering source terms are zero. With these assumptions, inner iterations described above are performed by fixing the ordinate direction (μ_m, ξ_m, η_m) and visiting all nodes in the computational domain. Once all ordinate directions have been scanned, the solution wall fluxes and source terms are recomputed. Iterations are continued until convergence has been achieved. Outer iterations can be performed to model spectral effects of the radiation and global iterations can be performed with an energy balance.

Solution Stability

When the cell-center intensity predicted from Eq. (24) is used with Eq. (25) to extrapolate the face intensity, the predicted face intensity may be negative, which is physically unrealistic. Usually, the negative intensities are set to zero[11] and the computations are continued. The knowledge of conditions to maintain positive intensities in the computational grid would certainly assist in minimizing spatial oscillations or in avoiding unstable conditions.

In Eq. (24), unstable conditions can occur when the terms in the numerator become negative. Stable solutions will be obtained using Eqs. (24) and (25) when the computational grid, local radiative conditions, and finite-difference methods satisfy the conditions,

$$\Delta x < \frac{|\mu|}{\beta(1-\alpha)}, \qquad \Delta y < \frac{|\xi|}{\beta(1-\alpha)}, \qquad \Delta z < \frac{|\eta|}{\beta(1-\alpha)} \tag{26}$$

Some local intensities may remain negative; these can be set to zero. Although the solutions are stable, spatial oscillations in the intensity can occur from the few local intensities that are zero. The conditions to maintain positive intensities and avoid unwanted oscillations throughout the computational grid can be written as

$$\Delta x < \frac{|\mu|}{\beta(1-\alpha)}\phi, \qquad \Delta y < \frac{|\xi|}{\beta(1-\alpha)}\phi,$$

$$\Delta z < \frac{|\eta|}{\beta(1-\alpha)}\phi \tag{27}$$

where

$$\phi = \frac{\alpha^3 + (1-\alpha)^2(2-5\alpha)}{\alpha}$$

If the computational grid is chosen to satisfy these constraints, physically unrealistic, negative intensities will not occur. A value of $\alpha = 1.0$ produces stable solutions regardless of the ordinate set chosen or the local radiative properties.

Equations (26) and (27) are conservative, because they neglect terms in the RTE that can effect positive intensity (volumetric emission, combustion sources, etc.). Since many times there are limitations on computing time and computer memory, it may not be practical to satisfy Eq. (27) (for $\alpha = 0.5$ and Δx, Δz, and $\Delta z = 0.0$). Instead, choose the grid fine enough to minimize the number of negative intensities that are obtained.

Ordinate Directions

The ordinates and weights used in the calculations are those proposed by Lathrop and Carlson.[17] The ordinate values are symmetric and the weights sum to 4π. These quadrature sets are constructed to be invariant under any 90 deg rotation and to satisfy a number of key moments of the radiative intensity:

1) Zeroth moment full range $0 \leq \Theta \leq \pi$ $\quad 0 \leq \phi \leq 2\pi$

2) First moment half range $0 \leq \Theta \leq \pi/2$† $\quad 0 \leq \phi \leq 2\pi$

3) First moment full range $0 \leq \Theta \leq \pi$ $\quad 0 \leq \phi \leq 2\pi$

The need to satisfy the key moments was documented in Ref. 20; otherwise, incorrect boundary heat fluxes will result, leading to improper prediction of boundary temperatures. The quadrature ordinates and weights for the first several SN approximations are listed in Table 1 for the first quadrant.

Table 1 SN quadrature[17] for the first quadrant

Approx.	SN point	Ordinates μ	ξ	η	Weights w
S2	1	0.5773503	0.5773503	0.5773503	1.5707963
S4	1	0.2958759	0.2958759	0.9082483	0.5235987
	2	0.9082483	0.2958759	0.2958759	0.5235987
	3	0.2958759	0.9082483	0.2958759	0.5235987
S6	1	0.1838670	0.1838670	0.9656013	0.1609517
	2	0.6950514	0.1838670	0.6950514	0.3626469
	3	0.9656013	0.1838670	0.1838670	0.1609517
	4	0.1838670	0.6950514	0.6950514	0.3626469
	5	0.6950514	0.6950514	0.1838670	0.3626469
	6	0.1838670	0.9656013	0.1838670	0.1609517
S8	1	0.1422555	0.1422555	0.9795543	0.1712359
	2	0.5773503	0.1422555	0.8040087	0.0992284
	3	0.8040087	0.1422555	0.5773503	0.0992284
	4	0.9795543	0.1422555	0.1422555	0.1712359
	5	0.1422555	0.5773503	0.8040087	0.0992284
	6	0.5773503	0.5773503	0.5773503	0.4617179
	7	0.8040087	0.5773503	0.1422555	0.0992284
	8	0.1422555	0.8040087	0.5773503	0.0992284
	9	0.5773503	0.8040087	0.1422555	0.0992284
	10	0.1422555	0.9795543	0.1422555	0.1712359

†Except S2 approximation.

Results

The radiative transport equation is iteratively solved with the steady energy equation in which the convection and conduction are assumed negligible,

$$\nabla \cdot q_R = S \tag{28}$$

The divergence of the radiative flux $\nabla \cdot q_R$ is found by integrating the RTE over all Ω directions,

$$-\nabla \cdot q_R = \kappa(G - 4E_g) \tag{29}$$

and the parameter S represents the heat source. Convergence is achieved when the maximum residual of the incident energy is less than a preset error. Solutions are tested by varying the number of control volumes and the level of error to ensure a converged solution. A radiative balance is computed equating net flux deposited on the bounding walls with energy deposited in the volumes. The discrete-ordinates method was found to balance, implying that the radiative energy is conserved.

Exact solutions were used whenever possible to benchmark the method. Crosbie[4,5] has established the mathematical relations for an exact solution in a simple three-dimensional cubical enclosure. The emissive power at the center of the cube was shown to be the average of the six surface emissive powers. Although discrete-ordinate solutions for a first-order method ($\alpha = 1.0$) always satisfied this constraint (to six digits), the diamond-difference solutions ($\alpha = 0.5$) deviated somewhat ($< 10\%$), yet were more accurate when the solution errors were examined for the entire solution domain.

One of the difficulties with the analysis of three-dimensional applications is the sheer mass of numbers that need to be analyzed and presented. Unfortunately, only a sample of the results obtained can be presented.

Absorbing Medium

A unit cubical enclosure depicted in Fig. 1 is studied, since the discrete-ordinates method can be benchmarked against the numerically exact solution in Ref. 7. Discrete-ordinate solutions were found for S2, S4, S6, and S8 approximations, which correspond to 8, 24, 48, and 80 flux approximations using the ordinate values summarized in Table 1. Two finite-difference schemes were considered: the second-order-accurate, diamond-difference scheme[12] ($\alpha = 0.5$), and a first-order-accurate method ($\alpha = 1.0$). Solutions were found for computational grids of 125 control volumes ($5 \times 5 \times 5$) and 1331 control volumes ($11 \times 11 \times 11$). Convergence was based on a preset error of 0.01% on the incident energy, unless otherwise noted.

The walls of the enclosure are considered radiatively black ($\epsilon = 1$), with unit emissive powers at $x = 1$, $y = 0$, and $z = 0$ and zero emissive powers on the other walls. The medium is in radiative equilibrium, with an extinction coefficient of $\kappa = 1.0$ m^{-1}. Figures 3 and 4 show the predicted emissive power at the $z = 0.5$ m and $z = 0.9$ m planes for the two finite-difference approximations, compared with the exact solution of Larsen.[7] The surface heat flux for $z = 1.0$ m is shown in Fig. 5 and is compared with the exact solution. The maximum solution errors occur at $z = 1$ in the corner near $x = 0$ and $y = 1$. The discrete-ordinate solutions for the diamond-difference method compare better with the exact solution than the first-order, finite-difference method.

Maximum and average errors computed between the discrete-ordinates method and the zone method[7] are plotted in Fig. 6 for the S2–S8 flux approximations. Solution errors are compared for two finite-difference schemes and results are shown for the emissive power at planes $z = 0.5$ and 0.9 m and the wall heat flux at $z = 1.0$ m. In general, the average error decreases as the number of fluxes is increased. The eight-flux (S2) approximation for low-order SN is inaccurate. The diamond-difference scheme is, on average, more accurate for the ordinate approximations S4, S6, and S8.

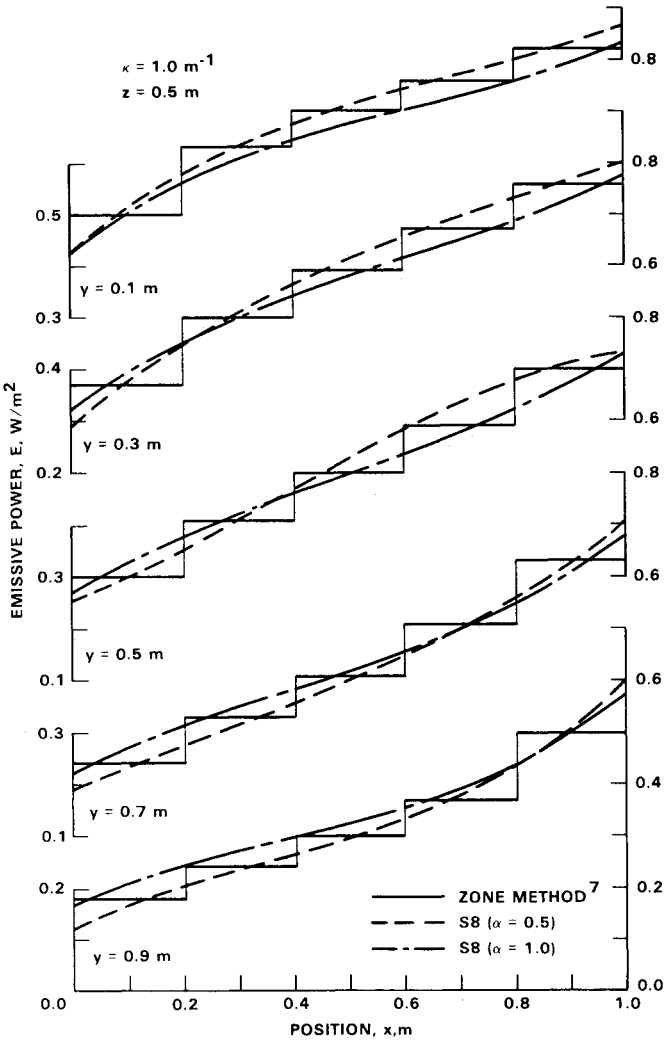

Fig. 3 Comparison between the discrete-ordinate and zone methods[7] for emissive power at the plane, $z = 0.5$ m.

For an absorption coefficient of unity, the discrete-ordinates method requires approximately 0.00022 CPU s/iteration-node-direction using a VAX 11/785 digital computer. The iterations needed to achieve a converged solution with a preset error were independent of the grid size (a $5 \times 5 \times 5$ or $11 \times 11 \times 11$ computational grid). The error was measured as a maximum relative residual of the incident energy and can be approximated as

$$\epsilon \simeq 1.5e^{-i}$$

with i denoting the number of iterations. This equation also implies the rate of convergence was identical for both grids. The required iterations to achieve a converged solution with a fixed 0.01% error were found to vary with the absorption coefficient as follows

$$i = 11\kappa^{0.57}$$

for the range $0.1 \leq \kappa \leq 10$. The converged solutions were found to be independent of flux or difference approximation. For example, it takes 10 to 11 iterations with $\kappa = 1.0$ m^{-1} for a level of error of 0.01%, regardless of SN approximation (S2, S4, S6, or S8), difference approximation ($\alpha = 0.5$ or $\alpha = 1.0$), or computational grid ($5 \times 5 \times 5$ or $11 \times 11 \times 11$). The iteration-by-iteration estimates of the source term were found to limit the rate of convergence.

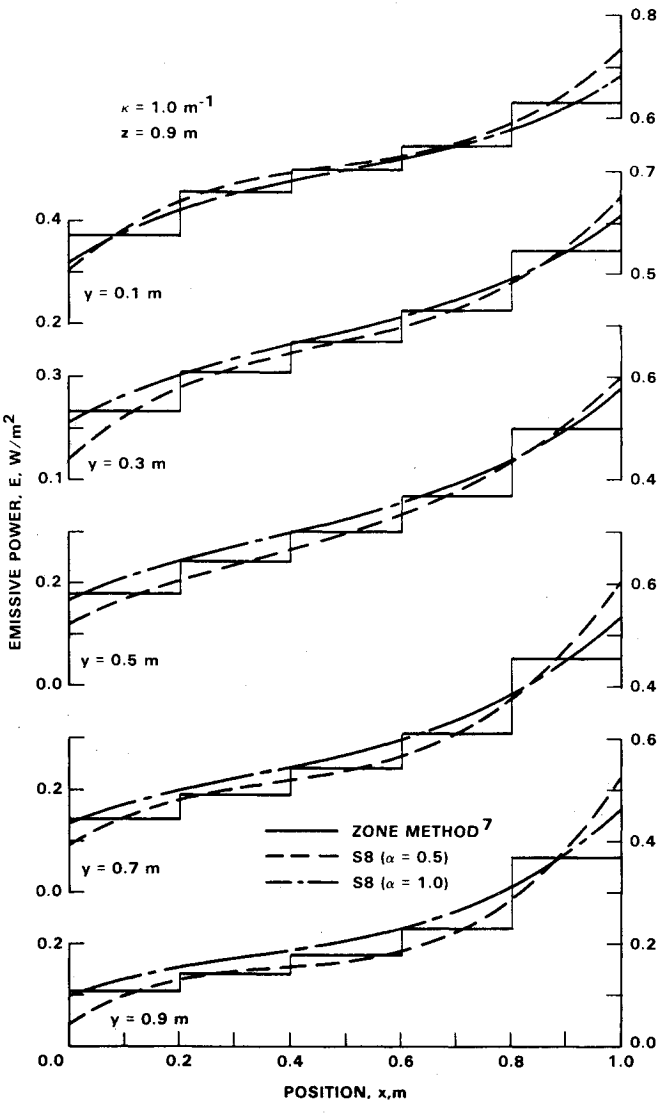

Fig. 4 Comparison between the discrete-ordinate and zone methods[7] for emissive power at the plane, $z = 0.9$ m.

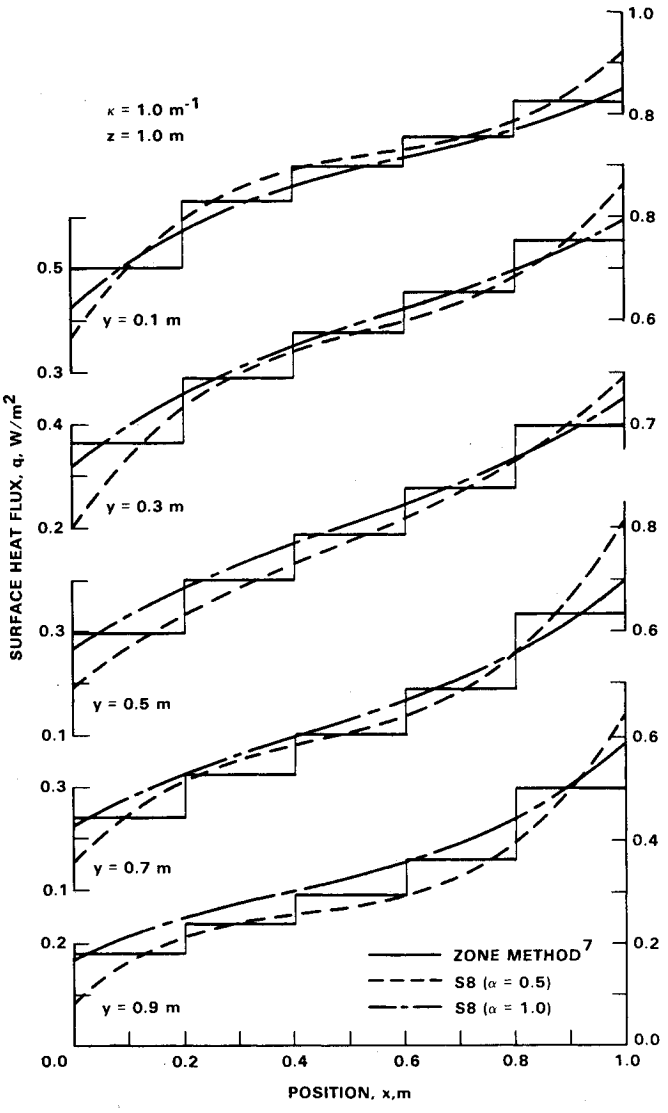

Fig. 5 Comparison between the discrete-ordinate and zone methods[7] for net surface heat flux at the wall, $z = 1.0$ m.

Following Menguc and Viskanta,[9] an idealized furnace is modeled using the discrete-ordinates method with the diamond-difference approximation ($\alpha = 0.5$). The S4, S6, and S8 predictions are compared with the P3 approximation and the exact solution. The computational domain for the system under consideration is shown in Fig. 1. Menguc and Viskanta[9] listed the following data for the medium:

$$\kappa = 0.5 \text{ m}^{-1} \qquad S = 5.0 \text{ kW/m}^3$$

the geometry:

$$L_x = 2 \text{ m} \qquad L_y = 2 \text{ m} \qquad L_z = 4 \text{ m}$$

and the boundaries:

$z = 0$	$T = 1200$ K	$\epsilon = 0.85$
$z = L_z$	$T = 400$ K	$\epsilon = 0.70$
others	$T = 900$ K	$\epsilon = 0.70$

Predictions were obtained using the $7 \times 7 \times 11$ nonuniform grid suggested by Menguc and Viskanta.[9]

In Fig. 7, the predicted temperature distributions are shown for three axial locations in the furnace and are compared with the P3 approximation and Hottel's zone method. Near the hot wall ($z = 0.4$ m), the S4, S6, and S8 approximations are slightly less accurate (< 0.5%) than the P3 method. At the center of the furnace, the S6 and S8 solutions are within 1% of the zone solution and are comparable with the P3 approximation. The S4 solution is within 2.0% of the exact solution. At the cold wall ($z = 3.60$ m), the maximum errors between the exact and the S4, S6, and S8 solutions are < 1.0%, while the error in the P3 approximation is about 2.3%. The deviations were found to decrease with increasing optical thickness. For example, the S4, S6, and S8 discrete-ordinate predictions are within 0.5% of the exact solution for the same enclosure with an absorption coefficient of $\kappa = 1.0$ m^{-1} in the medium, while the P3 approximation is within 1.5% of the exact solution.

The predicted heat fluxes at the hot and cold surfaces using the S4, S6, and S8 discrete-ordinate approximations are compared in Fig. 8 with values from the exact-zone method and the P3 approximation. For $\kappa = 0.5$ m^{-1}, the S4 and S6 predictions for the net surface radiant fluxes are within 3.0% at the hot face and within 4.0% at the cold face of the exact solution, while the S8 approximation is within 2.0% at the hot and cold faces. Discrete-ordinates predictions are in considerably better agreement with the exact solution than the P3 predictions, which only estimates the surface heat fluxes within 20% at the hot and cold faces.

Menguc and Viskanta[9] quoted computer run times of 35–40 min on a VAX 11/780 for the $7 \times 7 \times 11$ grid. The S4 discrete-ordinates solution required 31 s for the same grid, 11

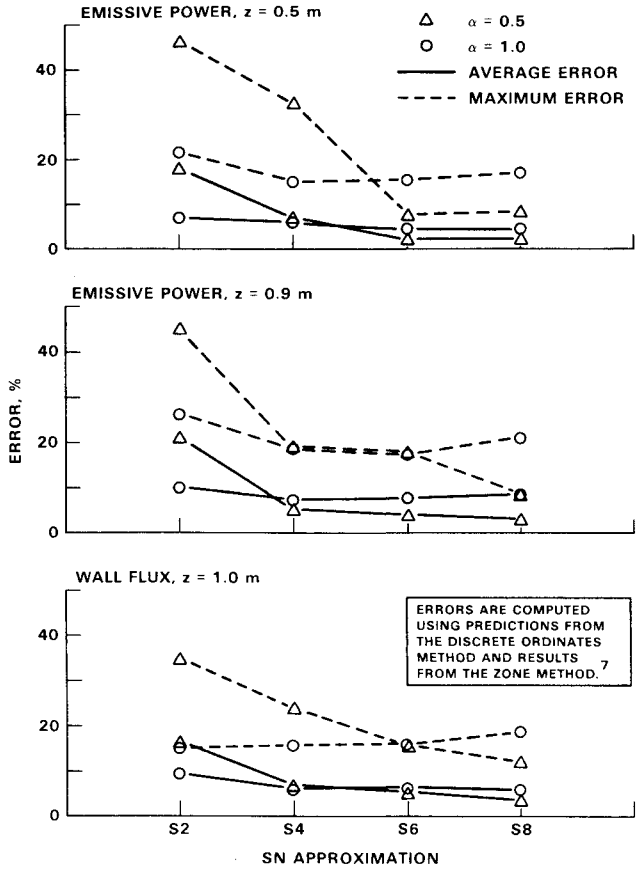

Fig. 6 Comparison between two finite-difference solutions for a number of discrete-ordinate approximations.

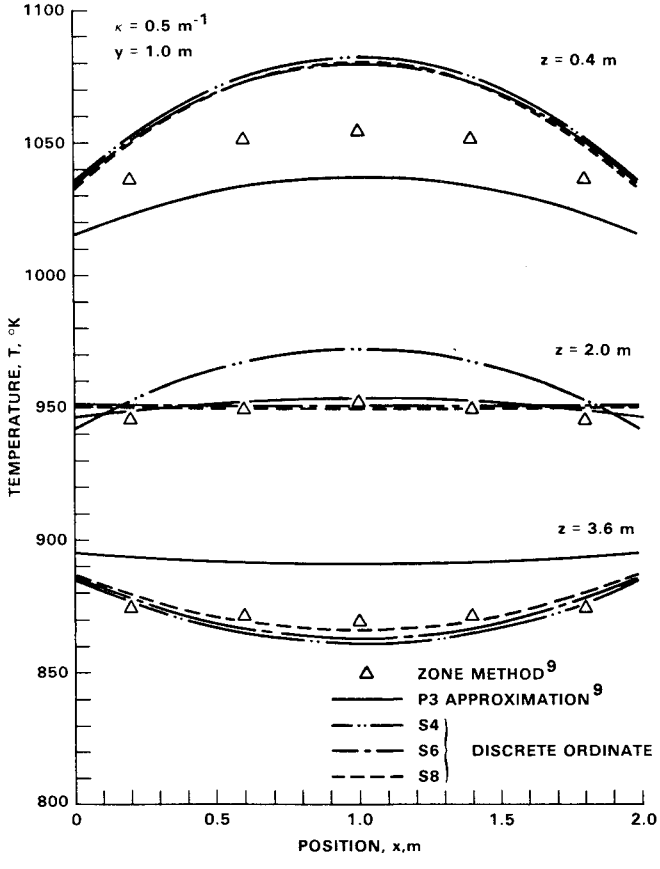

Fig. 7 Comparison between the discrete-ordinates solutions, the P3 approximation, and the zone method[9] for temperature distributions at three axial locations ($z = 0.4$, 2.0, and 3.6 m).

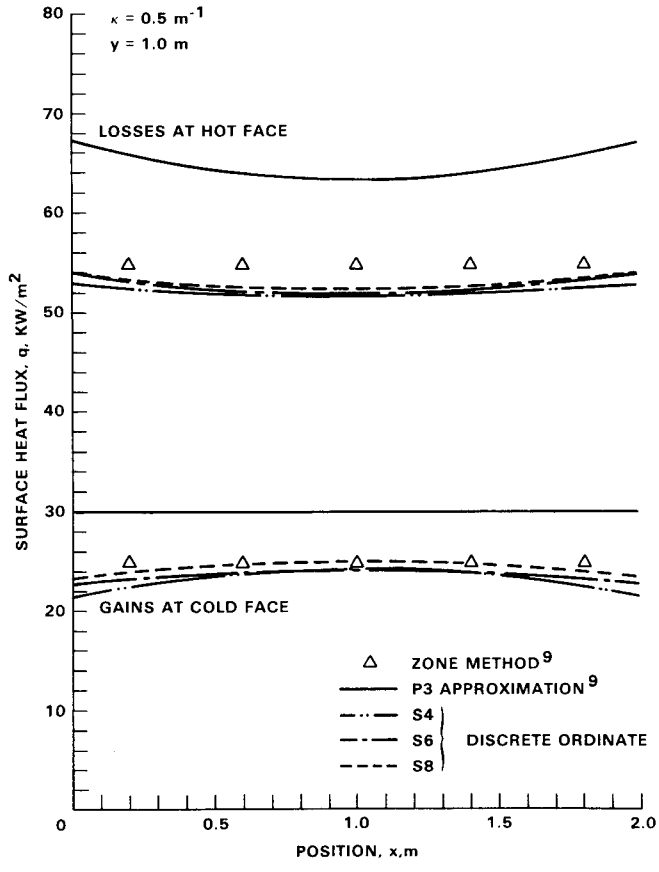

Fig. 8 Comparison between the discrete-ordinates solutions, the P3 approximation, and the zone method[9] for surface heat flux at the hot and cold walls.

iterations, and an error in the incident energy of 0.01%. An S8 approximation required about 90 s to run.

Scattering Medium

The discrete-ordinates method can also be applied to enclosures with scattering media. Consider the cubical enclosure in radiative equilibrium that was studied in this paper and by Larsen.[7] Equation (29) was substituted into the RTE and a scattering problem was solved. The attenuation coefficients, $\sigma = 1.0\ \text{m}^{-1}$ and $\kappa = 0.0\ \text{m}^{-1}$, were used, and the same results quoted in Figs. 3–5 were obtained. The same strategy was followed for the idealized furnace studied by Menguc and Viskanta.[9] The form of the radiative transport equation is identical to Eq. (1) in addition to an isotropic source term from the source of combustion S. Predictions were obtained using attenuation coefficients of $\sigma = 0.5\ \text{m}^{-1}$ and $\kappa = 0.0\ \text{m}^{-1}$ with the combustion source, $S = 5.0\ \text{kW/m}^3$. The same results quoted in Figs. 7 and 8 were obtained.

For most applications, the medium scatters anisotropically and Eq. (8) must be solved simultaneously with Eq. (29). As an example, consider several of the phase functions studied in Ref. 9,

Case 1: $f = 0$	$g = 0$
Case 2: $f = 0.111$	$g = 0.215$
Case 3: $f = 0.781$	$g = 0.868$

where the parameters f and $b_1 = g$ are those defined in Eq. (5). The following conditions in the furnace were assumed: $\epsilon = 0.8$ for all walls, $\sigma = 0.5\ \text{m}^{-1}$, and $\kappa = 0.5\ \text{m}^{-1}$. Figure 9 summarizes the S4 predictions for the net surface heat flux at the hot ($z = 0$ m) and cold ($z = 4$ m) walls. Increasing the forward scatter increases the net surface losses at the hot face and the net gains at the cold face. In addition, as the forward

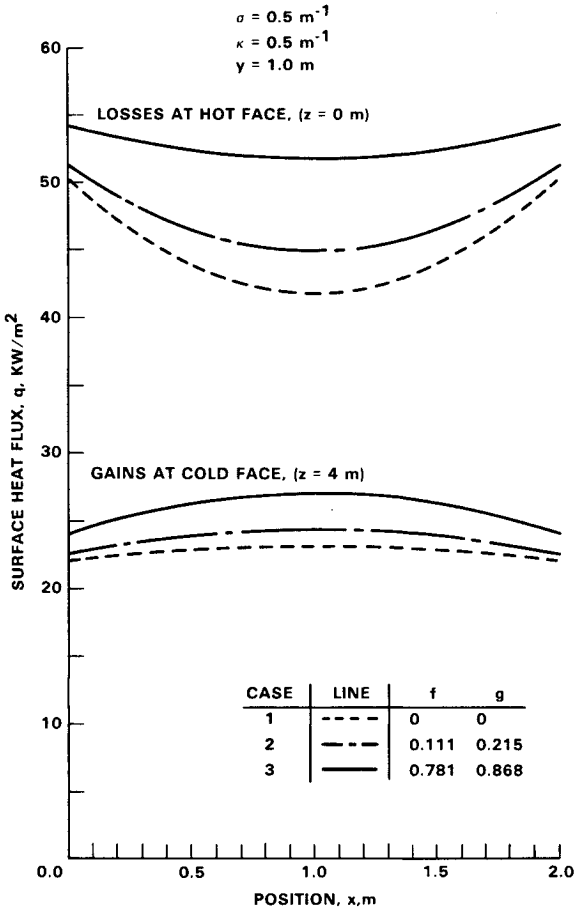

Fig. 9 Predicted surface heat flux at hot and cold walls for several phase functions.

scattering is increased, the gradient in heat flux is reduced on the hot face and increased on the cold face.

Conclusion

A three-dimensional radiative heat-transfer model based on the discrete-ordinates method has been developed. The method presented in this paper can be used to solve for the three-dimensional distributions of radiative intensity, incident energy, and wall heat flux. Solution stability can be maintained using the conditions listed in the paper. The method is easily applied to a number of higher-order approximations (8, 24, 48, and 80 fluxes) that simulate the continuous distribution of radiant flux and is easily applied to several finite-difference approximations. The work indicates the S2 approximation is too inaccurate to use. The S4 approximation yields reasonable results for the amount of numerical work and is recommended for use, while the S6 and S8 approximations require considerably more numerical effort and their use may be harder to justify. The discrete-ordinates model can simulate gray walls and anisotropic scattering and was found to accurately predict radiant heat transfer for two test enclosures, to efficiently converge to the solutions, and to easily permit changes in the computational grid that are necessary if the method is to be compatible with other finite-difference schemes.

References

[1]Smoot, L.D. and Smith, P.J., *Coal Combustion and Gasification*, Plenum Press, New York, 1985.

[2]Fiveland, W.A. and Wessel, R.A., "A Numerical Model for Predicting Performance of Three-Dimensional Pulverized Fuel Fired Furnaces," ASME Paper 86-HT-35, June 1986.

[3]Viskanta, R., "Radiative Heat Transfer," *Fortschritte der Verfahrenstechnik*, Vol. 22, 1984, pp. 51–81.

[4]Crosbie, A.L. and Schrenker, R.G., "Exact Expressions for Radiative Transfer in a Three-Dimensional Rectangular Geometry," *Journal of Quantitative Spectroscopy and Radiative Transfer*, Vol. 28, 1982, pp. 507–526.

[5]Crosbie, A.L. and Schrenker, R.G., "Radiative Transfer in a Two-Dimensional Rectangular Medium Exposed to Diffuse Radiation," *Journal of Quantitative Spectroscopy and Radiative Transfer*, Vol. 31, 1984.

[6]Howell, J.R., "Application of Monte Carlo to Heat Transfer Problems," *Advances in Heat Transfer*, Vol. 5, edited by T.F. Irvine, Jr. and J.P. Hartnett, Academic Press, New York, 1968, pp. 1–54.

[7]Larsen, M.E., "Exchange Factor Method and Alternative Zonal Formulation for Analysis of Radiating Enclosures Containing Participating Media," Ph.D. Thesis, University of Texas, Austin, 1983.

[8]Lockwood, F.C. and Shah, N.G., "New Radiation Solution Method for Incorporation in General Combustion Prediction Procedures," *Proceedings of Eighteenth Symposium (International) on Combustion*, The Combustion Institute, Pittsburgh, 1981, pp. 1405–1414.

[9]Menguc, M. and Viskanta, R., "Radiative Transfer in Three-Dimensional Rectangular Enclosures," *Journal of Quantum Spectroscopy and Radiative Transfer*, Vol. 33, 1985, pp. 533–549.

[10]Chandrasekhar, S., *Radiative Transfer*, Oxford at Clarendon Press, London, 1950.

[11]Carlson, B.G. and Lathrop, K.D., *Transport Theory—The Method of Discrete-Ordinates in Computing Methods in Reactor Physics*, edited by H. Greenspan, C. Kelber, and D. Okrent, Gordon and Breach, New York, 1968.

[12]Lathrop, K.D., "Use of Discrete-Ordinate Methods for Solution of Photon Transport Problems," *Nuclear Science and Engineering*, Vol. 24, 1966, pp. 381–388.

[13]Khalil E. and Truelove, J., "Calculation of Radiative Heat Transfer in a Large Gas Fired Furnace," *Letters in Heat and Mass Transfer*, Vol. 4, Pergamon Press, 1977, pp. 353–365.

[14]Fiveland, W.A., "A Discrete-Ordinates Method for Predicting Radiative Heat Transfer in Axisymmetric Enclosures," ASME Paper 82-HT-20, 1982.

[15]Fiveland, W.A., "Discrete-Ordinates Solutions of the Radiative Transport Equation for Rectangular Enclosures," *Transactions of ASME, Journal of Heat Transfer*, Vol. 106, 1984, pp. 699–706.

[16]Lathrop, K.D., "THREETRAN: A Program to Solve the Multigroup Discrete-Ordinates Transport Equation in (x,y,z) Geometry," Los Alamos Scientific Laboratory, Los Alamos, NM, Repts. UC-32 and UC-79, May 1976.

[17]Lathrop, K. and Carlson, B., "Discrete-Ordinates Angular Quadrature of the Neutron Transport Equation," Los Alamos Scientific Laboratory, Los Alamos, NM, Rept. LASL-3186, 1965.

[18]Wiscombe, W.J., "The Delta-M Method. Rapid Yet Accurate Radiative Flux Calculations for Strongly Asymmetric Phase Functions," *Journal of Atmosphere Sciences*, Vol. 34, 1977, pp. 1408–1422.

[19]Joseph, J.H., Wiscombe, W.J., and Weinman, J.A., "The Delta-Eddington Approximation for Radiative Flux Transfer," *Journal of Atmospheric Sciences*, Vol. 33, 1976, pp. 2452–2459.

[20]Fiveland, W.A., "Discrete-Ordinate Methods for Radiative Heat Transfer in Isotropically and Anisotropically Scattering Media," *Journal of Heat Transfer*, Vol. 109, 1987, pp. 809–812.